

Synthesis and Characterization of a Highly Electroactive Composite Based on Au Nanoparticles Supported on Nanoporous Activated Carbon for Electrocatalysis

Giulia Moggia,^{*[a, b, c]} Saskia Hoekx,^[b, d] Nick Daems,^[b] Sara Bals,^[d] and Tom Breugelmanns^[b]

A facile, "one-pot", chemical approach to synthesize gold-based nanoparticles finely dispersed on porous activated carbon (Norit) was demonstrated in this work. The pH of the synthesis bath played a critical role in determining the optimal gold-carbon interaction, which enabled a successful deposition of the gold nanoparticles onto the carbon matrix with a maximized metal utilization of 93%. The obtained AuNP/C nanocomposite was characterized using SEM, HAADF-STEM electron tomography and electrochemical techniques. It was found that the Au nanoparticles, with diameters between 5 and 20 nm, were evenly distributed over the carbon matrix, both inside and outside the pores. Electrochemical characterization indicated that the composite had a very large electroactive

surface area (EASA), as high as 282.4 m² g_{Au}⁻¹. By exploiting its very high EASA, the catalyst was intended to boost the productivity of glucaric acid in the electrooxidation of its precursor, gluconic acid. However, cyclic voltammetry experiments revealed a very limited reactivity towards gluconic acid oxidation, due to the spacial hindrance of gluconic acid molecule which prevented diffusion inside the catalyst nanopores. On the other hand, the as-synthesized nanocomposite promises to be effective towards the ORR, and might thus find potential application as anode catalyst for fuel cells as well as for the scalability of all those electrochemical reactions involving small molecules with high diffusivity and catalysed by noble metals (i.e. CO₂, CH₄, N₂, etc.).

Introduction

Recent advances in supported metal nanoparticles (NPs) have opened the doors to new opportunities towards catalytic systems with enhanced electrocatalytic activity through superior surface properties, amongst others finding applications in energy storage, sensors and also in electrocatalytic conversion.^[1–4] In fact, the use of nanomaterials allows to boost the electrochemical performance as a consequence of the

increased surface-to-volume ratio while keeping the utilized amount of the often expensive active phases limited.^[5,6,15,7–14]

Amongst these newly developed metal electrocatalysts, gold-based nanoparticles (AuNPs) have proven to be particularly promising thanks to their stability and versatility.^[16] In fact, they have shown great potential in many electrocatalytic applications,^[16] like the electrocatalytic oxidation of small organic molecules (e.g., methanol, ethanol, formic acid), thanks to their excellent catalytic activity, selectivity and good resistance to CO poisoning,^[17–19] fuel cells,^[20–22] in the ORR in alkaline media,^[23–29] and the electrochemical reduction of CO₂^[30–32] and N₂.^[33–36]

Common AuNPs synthesis methods include: the Turkevich method, colloidal methods, galvanic replacement, soft template methods, dealloying, template synthesis, hydrothermal-assisted growth, and electrochemical deposition.^[37–47] Due to the larger surface-to-volume ratio (and more electrocatalytic active sites), AuNPs show better activity in electrocatalysis than bulk Au.^[16] Moreover, composition and morphology also play a role in their electrocatalytic performance. For instance, when combined with other elements (e.g., Ag, Pd, Cu, Ir, and Pt), the synergistic effect of different elements can enhance the catalytic performance of AuNPs.^[48–52] Similarly, the morphology of Au nanomaterials also affects their electrocatalytic performance.^[53,54] For example, Au-based nanomaterials with various architectures have been successfully synthesized, such as nanowires,^[55] nanorods,^[56] nanodendrites,^[57] and nanocages,^[58] where shape, structure, and interface of noble metal can be optimized to significantly improve their catalytic properties. In many electrocatalytic applications, the leverage of a support also plays a role in the overall catalyst performance, for example, by helping to

[a] G. Moggia

Present address:

Climate, Infrastructure and Environment Executive Agency of the European Commission,
Chaussée de Wavre 910, 1040 Etterbeek, Brussels, Belgium

[b] G. Moggia, S. Hoekx, Dr. N. Daems, Prof. Dr. T. Breugelmanns

Research group Applied Electrochemistry & Catalysis,
University of Antwerp,
Universiteitsplein 1, 2610 Wilrijk, Belgium
E-mail: giulia.moggia@student.uantwerpen.be

[c] G. Moggia

Separation & Conversion Technologies,
Flemish Institute for Technological Research (VITO),
Boeretang 200, 2400 Mol, Belgium

[d] S. Hoekx, Prof. Dr. S. Bals

Research group Electron Microscopy for materials science,
University of Antwerp,
Groenenborgerlaan 171, 2020 Antwerp, Belgium

 Supporting information for this article is available on the WWW under <https://doi.org/10.1002/celec.202300293>

 © 2023 The Authors. ChemElectroChem published by Wiley-VCH GmbH. This is an open access article under the terms of the Creative Commons Attribution License, which permits use, distribution and reproduction in any medium, provided the original work is properly cited.

prevent the aggregation of the NPs thus improving the catalyst durability.^[16,59] Moreover, some literature studies report synergistic effects between nanoparticles and support which result in improved catalytic activity of the composite compared to the nanoparticles or support materials alone.^[59–62] Despite many AuNPs-based catalysts have been reported and have shown good electrocatalytic properties, their electrocatalytic activity is still unsatisfactory for potential use in larger-scale applications.

In this context, nanoporous noble metal composites have received increasing interest in recent years for their excellent electrocatalytic activity, due to their very high electro-active surface areas (EASAs).^[63–65] However, the obtained mass-specific electroactive surface areas are still very limited (typically below $40 \text{ m}^2 \text{ g}^{-1}$) and the catalytic activity can still be improved.^[63] Hence, the development of nanoporous noble metal electrodes with high EASA and a high noble metal utilization efficiency remains a field of great interest and importance.

In this work, we developed a facile, one-pot chemical method to synthesize a AuNPs-based catalyst with very high electroactive surface area and, at the same time, low Au loading. The prepared catalyst consists of AuNPs ranged between 5 and 20 nm, evenly deposited over a nanoporous activated carbon (AC) matrix, exhibiting a specific EASA as high as $282.43 \text{ m}^2 \text{ g}_{\text{Au}}^{-1}$, which is 10^2 times higher than that found for the Au bulk RDE used for our previous studies (39.5 cm^2 vs. 0.702 cm^2). In our recent works, we have proven the capacity of bulk Au electrodes to selectively oxidize glucose to gluconic acid and gluconic acid to glucaric acid in alkaline media.^[66,67] However, such electrodes are characterized by very limited electrocatalytic activity as well as susceptibility to poisoning. The aim of this work was to boost the catalyst surface-to-volume ratio, as such allowing to achieve higher electrocatalytic activity (and glucaric acid productivity) with lower total metal loading, as well as stabilizing the Au nanoparticles on a carbon support in an attempt to address the issue caused by the physical blockage of the catalyst active sites and maintain a high activity.^[66–73]

Experimental

Chemicals and reagents

The synthesis bath was prepared using tetrachloroauric acid trihydrate (Sigma-Aldrich, 99%), ultrapure water (Synergy UV system), sodium hydroxide (Sigma-Aldrich, 98%), Polyvinylpyrrolidone (PVP40) (Sigma Aldrich), activated carbon Norit® SX1G (Total surface area, BET, $1000 \text{ m}^2 \text{ g}^{-1}$, Nederland BV.^[74]), used as received, and sodium borohydride (Sigma Aldrich, 98%). The ink was prepared using 2-propanol (ChemLab, >99%) as solvent and Sustanion® (suspension of 5 wt% in lower aliphatic alcohols and water), purchased from Sigma Aldrich, as solvent. The supporting electrolytes were prepared with ultrapure water (Synergy UV system), sodium carbonate (Sigma-Aldrich, 98%) and sodium hydroxide (Sigma-Aldrich, 98%). Anhydrous D-glucose was purchased from VWR (99.5%), D-gluconic acid potassium salt (98%) and D-saccharic acid potassium salt (98%) from Sigma Aldrich and D-gluconic acid sodium salt (99%) from Acros Organics. All chemicals were used without further modifications.

Preparation of AuNPs supported on activated carbon

The catalyst was prepared using a modification of the wet impregnation method developed by Hermans et al.^[75–77] (Figure 1). 30 mg $\text{HAuCl}_4 \cdot 3\text{H}_2\text{O}$ was dissolved in 150 mL MilliQ water under stirring at 600 rpm and ambient temperature (solution 1). The pH of the solution was adjusted to the target value (9–11) by adding an appropriate amount of a 1 M NaOH solution. Polyvinylpyrrolidone (PVP) was added from a 2%wt solution in order to obtain a concentration of $64 \mu\text{g mL}^{-1}$ in the final solution. PVP was used as stabilizing agent and, according to a previous study of our group, is expected to decrease the electrochemical charge transfer resistance and increase the electrochemically active surface area.^[78] Then, 150 mL of a solution obtained dissolving 135 mg of activated carbon (Norit) in MilliQ water (pH corrected with 1 M NaOH to target: 9 to 11) was added to solution 1. The resulting solution (solution 2) was left under stirring for 24 h. Following, a 0.1 M NaBH_4 (the reducing agent) solution was added dropwise to solution 2 such that the concentration of NaBH_4 in the final solution matched the one of Au. The solution was left under stirring (600 rpm) for 2 h (immobilization time). After this time, the slurry was filtered and washed with water six times to remove all the Cl^- . To verify that all the Cl^- had been removed, AgNO_3 was added to the filtrate to check for the absence of precipitate. The catalyst was then dried in an oven at 70°C for 5 h and calcined at 200°C for 3 h. The whole synthesis process has been conducted under Argon to avoid alteration of the pH due to the presence of CO_2 .

Physical characterization of the AuNP/AC catalyst

The AuNP/C catalyst was investigated using a set of physicochemical characterization techniques.

Standards for all metallic species analyzed were purchased from VWR (Belgium). The Au weight percentage in the catalyst powders was analyzed by Thermo-gravimetric analysis (TGA), using a Q500 thermogravimetric analyzer (TA Instruments) and inductively coupled plasma mass spectrometry (ICP-MS), using an Agilent 7500 series spectrometer. For the TGA analysis, the temperature of the furnace was ramped from 40°C to 600°C – 800°C at $5^\circ\text{C}/\text{min}$. Platinum pans were used in all measurements. The Au wt.% was calculated from the residue at 600°C , which was found to be metallic Au by XRD analysis. To measure the Au content by ICP-MS analysis, 10 mg sample was dissolved in 500 μL of aqua regia and destructed at 70°C overnight. The samples were diluted to a 1:100

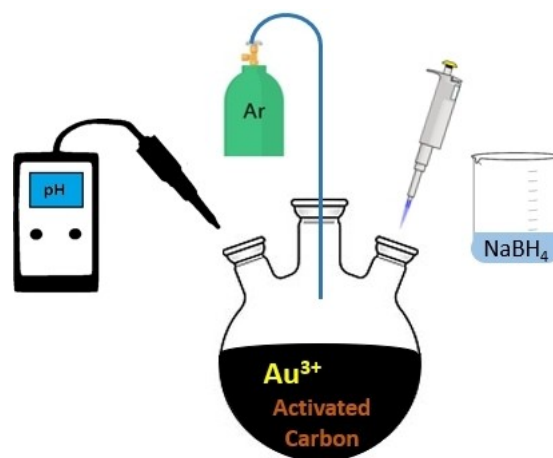


Figure 1. Schematic representation of the synthesis of AuNP/C catalyst by impregnation.

ratio and a calibration curve was fitted from 100 to 10 000 ppb. However, with this method the Au content (%wt.) measured was only 0.3%, too low compared to the theoretical one, given by the difference between the quantity of Au added during the synthesis and that left in the filtrate solution, and also compared to Au content measured by TGA. Matching results were only obtained when the samples of Au/C powder were carbonized prior to the ICP-MS analysis, thus eliminating the carbon matrix and leaving only the metal. The procedure used was the following: first, porcelain crucibles were pre-heated for 1 h in a muffle furnace at 700 °C. Crucibles were weighed after cooling; second, 50–100 mg of sample was placed in the crucible, weighted and placed in the muffle furnace for 4 h at 700 °C; third, after cooling, the crucible was weighted and the ash content was calculated. Ash was transferred to a falcon tube and digested in 1 mL of aqua regia overnight. Finally, the samples were diluted to perform the ICP-MS measurement.

Next, in order to characterize the crystalline structure of the catalysts, X-Ray diffraction (XRD) was employed. X-ray diffraction experiments were performed on a Huber X-ray diffractometer equipped with a G670 Guinier camera (Huber GmbH&Co, Germany) using the Cu K α 1 radiation ($\lambda = 1.5405981 \text{ \AA}$).

Scanning Electron Microscopy and Energy-dispersive X-Ray Spectroscopy (SEM-EDX) were used in order to assess the morphology and distribution of the metal nanoparticles over the carbon support. The microscope used was a Quanta 250 FEI operated at an acceleration voltage of 5 kV and equipped with a Super-X EDX detector to study the morphology of the obtained catalysts and verify the atomic distribution.

For more detailed characterization and to determine the 3D structure of the supported Au nanoparticles, HAADF-STEM electron tomography experiments were performed on a Thermo Fischer Tecnai Osiris microscope operated at 200 kV. Tilt series for the materials were acquired using incremental fast tomography between -75° and 75° with a 2° tilt increment and a frame time of 6 s.^[79] The projection images were acquired with a 50 pA beam current and image resolution of 1024×1024 pixels. The series were aligned using cross-correlation and the reconstructions were completed using the Expectation Maximization (EM) algorithm in the ASTRA Toolbox.^[80] To determine the composition of the materials, EDX maps were obtained using the Super-X detector on the Tecnai Osiris microscope. The maps were acquired for 8 minutes at a 50 pA beam current.

Nitrogen (N₂) physisorption was performed at 77 K with a Quantachrome Quadrasorb SI (Quantachrome Instruments, Boynton Beach, FL, USA) automated surface area & pore size analyzer. Prior to the measurements, all samples were degassed for 16 h at 200 °C. The specific surface area was calculated using the Brunauer-Emmet-Teller (BET) equation.

Electrochemical setups

A thermostated three-electrode glass cell was used for the EASA experiments and for the cyclic voltammetry study to screen the electro-reactivity of the catalyst in gluconic acid and blank solution. A silver-silver chloride electrode (Ag/AgCl) and a platinum wire were used as reference and counter electrodes, respectively. The working electrode used for the cyclic voltammetry experiments consisted of a glassy carbon RDE (Goodfellow) with an active diameter of 8 mm which was covered with 14 μL of catalyst ink deposited by drop-casting until a loading of ca 50 μg (0.099 mg cm^{-2}). The catalyst ink was prepared dispersing the catalyst powder (5 mg) in a (1000 mL) solution of 2-propanol and 20 wt% Sustanion, so that the ratio Sustanion/catalyst was 1/7.

Before the catalyst deposition, the surface of the glassy carbon electrode was carefully polished with aluminum (Φ 1, 0.3 and 0.05 μm) slurry on a polishing cloth and then sonicated in MilliQ water for 5 min. The electrochemical instrumentation consisted of a Bio-Logic VSP-300 Potentiostat. All the electrode activities are represented as current densities, utilizing the geometric area of the GC electrode as active area and with respect to the reversible hydrogen electrode (V_{RHE}). The cyclic voltammetry studies were conducted between 0 and 2.5 V_{RHE} at 50 mV/s at ambient temperature from solutions containing 0.1 M aqueous NaOH while stirring at 700 rpm. All the voltammograms shown correspond to the cycle once a stable state is reached. An initial solution containing 0.05 M of gluconic acid in 0.1 M NaOH (pH 13) was used for the electrolysis.

The continuous flow experiments were executed in an adapted micro flow cell (ElectroCell, Denmark), allowing to operate in a three-electrode mode (Figure 2).

A detailed description can be found in a previous work.^[81] A 10.2 cm^2 porous electrode (Titanium fiber felt, Fuel Cell Store) was used as anode. The ink was sprayed onto the microporous layer of the felt until a total loading of 2.45 mg cm^{-2} was reached. The ink was ultra-sonicated for 25 min prior to airbrushing. The anodic potential was controlled versus a leak-free Ag/AgCl reference anode (Innovative Instruments, Inc.) with a multichannel Autolab potentiostat M204 equipped with a 10 A booster. The catholyte and anolyte used were both 0.1 M aqueous NaOH. In both, the flow rate was kept at 20 mL min^{-1} with a multichannel peristaltic pump. A Nafion[®] 117 cation exchange membrane separated the two compartments. The system was operated in recirculation mode as shown in Figure 2 and the electrolyte volumes were 250 mL for both anolyte and catholyte. The reactor was operated in a vertical position with the electrolyte being fed from the bottom of the reactor and leaving at the top, while at room temperature and atmospheric pressure.

The products were analyzed by HPLC (Alliance 2695, Waters, USA) combined with an ionexclusion column (Shodex KC-811). A photodiode array (PDA) detector set to 210 nm was used to detect organic acids while a refractive index (RI) detector thermostated at 30 °C was used to detect glucose. A perchloric acid solution (0.1%) was used as the eluant for the HPLC analysis. Prior to analysis, 1 mL samples were acidified with 200 μL perchloric acid 6 M solution, sonicated and finally filtered.

All the electrode activities reported are represented with current densities (measured at the beginning of every electrolysis), utilizing the EASA as active area and with respect to the reversible hydrogen electrode (RHE). The tested potential vs. Ag/AgCl was converted into potential vs. RHE using the Nernst equation (Eq. (1)):

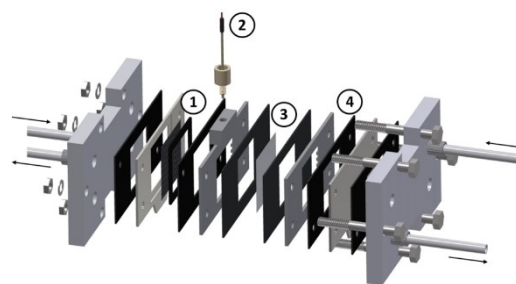


Figure 2. Scheme of the reactor setup used for the continuous flow experiments: (1) SS counter electrode (CE), in the cathodic compartment; (2) reference electrode (RE); (3) Nafion membrane and (4) anodic compartment containing the working electrode (WE).

$$E_{RHE} = E_{Ag/AgCl} + \ln(10) \cdot \frac{RT}{F} \cdot pH + 0.197 \quad (1)$$

With R being the universal gas constant ($8.314472 \text{ JK}^{-1} \text{ mol}^{-1}$), F the Faraday constant ($96485.332 \text{ C mol}^{-1}$) and T the temperature.

Electroactive surface area measurement

The electroactive surface area (EASA) of the synthesized catalyst was calculated using the capacitance, measured as the slope of the plot of the current vs. the scan rate (selected scan rates: 20, 40, 60, 80 and 100 mVs^{-1}) at 0.71 V_{RHE} in the electrolyte solution (0.1 M NaOH) (S1). To obtain the EASA, this value (i.e. 0.0131 F or $13100 \text{ } \mu\text{F}$) was divided by the value of capacitance of EDL for bulk gold found in literature,^[82] $14.25 \text{ } \mu\text{F cm}^{-2}$. The specific EASA, $282.4 \text{ m}^2 \text{ g}^{-1}$, was obtained by dividing the EASA, 919.3 cm^2 , by the quantity of gold in the catalyst, 0.0003255 g .

Results and Discussion

The AuNP catalysts were prepared on Norit activated carbon by a controlled adsorption method in which the interactions between the Au precursor and the carbonaceous support in aqueous solution were optimized by controlling the pH of the impregnation solution. In fact, the surface of the activated carbon presents different types of functional groups containing heteroatoms (O, N, and S),^[83] in varying amounts, which can be divided into acidic, neutral, and basic functions. This influences their surface characteristics and adsorption behavior. In particular, the carbon surface can be either positively or negatively charged in aqueous solution, depending on whether it is below or above a characteristic pH value, called the point of zero charge (PZC), which is equal to 9.0 for Norit carbon.^[84,85] At the pH corresponding to the PZC, the net overall surface charge would be zero; at $\text{pH} > \text{PZC}$, the negatively charged carbon surface attracts cations from solutions, while at $\text{pH} < \text{PZC}$, it attracts anions. Therefore, it is important to know at which pH the interactions between the metallic precursor and the carbonaceous support are maximized. For this reason, the synthesis of the Au/C catalyst was conducted at 4 different pH's, in the range 8–11.5, in order to identify at which pH, the maximum adsorption occurs. Figure S2 shows the thermogravimetric plots for 4 samples of catalysts obtained, respectively, from the synthesis conducted at pH 8.5, 9.5, 10.5 and 11.5. All the samples show a small mass loss (ca 5% wt.) from room temperature to around 100°C due to the evaporation of adsorbed water. Another slight weight loss (ca 5% wt.) is encountered between 300 and 350°C , which could be related to the decomposition of the residual polyvinylpyrrolidone (PVP) used as surfactant during the synthesis. The major mass loss (ca 75% wt.) between 400 and 800°C is attributed to the loss of the carbon support (Norit). The residual values shown in Figure S2 (b) represent the total amount of metallic composite in the catalyst samples. The Au loading was calculated by subtracting the residual mass of a blank Norit carbon sample (i.e., non-carbon contaminations, ca. 5.4%) from the total residual amount of metallic composite in the catalyst samples (Figure S2

(b)). In order to identify which species of gold was generated during the TG analysis, a sample of residual composite was analyzed by XRD, which revealed it was metallic gold. The resulting gold loading (Au% wt) was then plotted versus the pH in order to identify the pH at which the maximum adsorption occurs (Figure 3). To double-check the residual mass trends, the amount of non-adsorbed metal in solution – after filtration – was also determined by ICP-MS. As shown in Figure 3, the maximum adsorption of Au (9.3%) on the activated carbon occurs at a pH of 9.5, which is just above 9.0 (the PZC of Norit). The explanation for this is that, at a pH between 9 and 10, the carbon surface holds negative charges which attract the Au^{3+} cations from solution: the interaction between the Au precursor and the carbon support leads to the high loading. On the other hand, at $\text{pH} > 10$, the carbon surface is also negatively charged but the metal precursor, is less available due to its preferential complexation with OH^- at these conditions, leading to a weaker metallic precursor-carbon surface interaction and a lower loading. At $\text{pH} < 9$ the carbon surface is positively charged, so it attracts anions rather than cations from the solution, meaning that the interaction will be weak and the resulting loading low. For this reason, the optimal pH of 9.5, which resulted in the highest metal loading, was used to synthesize the AuNP/C catalyst used in the rest of this study. A similar behavior was observed by the authors Hermans et al. in the preparation of Au–Pd/C catalysts for glyoxal and glucose chemical oxidation.^[75–77]

Physical characterization of the catalyst

Samples of Au/C were characterized by XRD and SEM coupled with EDX. The crystallinity of the synthesized AuNPs was investigated by an X-ray diffraction (XRD) technique, and corresponding XRD patterns were shown in Figure 4. Gold nanocrystals exhibited four distinct peaks at $2\theta = 38.2^\circ$, 44.4° , 64.6° and 77.6° in the diffraction pattern, corresponding to (1 1 1), (2 0 0), (2 2 0) and (3 1 1) Bragg's reflection of face-centred-cubic (fcc) lattice (JCPDS no. 04–0784).^[86] The intense diffraction peak at 38.2 indicates that the preferred growth orientation of

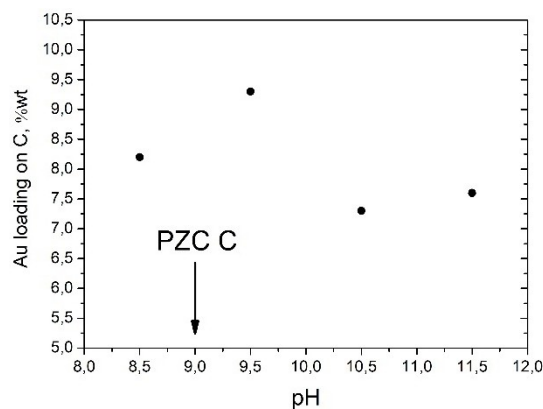


Figure 3. Au loading (% wt) on activated carbon, C, plotted versus the pH used for the synthesis. The point of zero charge for Norit® SX1G is ca 9.0.^[85]

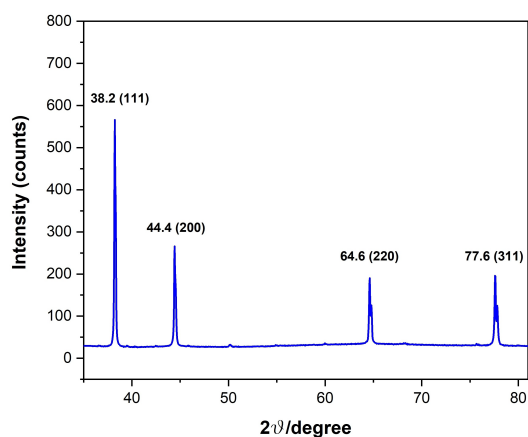


Figure 4. XRD pattern of the Au nanoparticles grown on activated carbon at optimized pH (9.5). The crystalline nanoparticles are represented by four peaks corresponding to standard Bragg reflections (111), (200), (220), and (311) of face centers cubic lattice. The intense peak at 38.2 represents preferential growth in the (111) direction.

zero-valent gold was fixed in the (111) direction.^[87] This XRD pattern is typical of pure Au nanoparticles.^[86,87]

The AuNP/C samples were further characterized by SEM and EDX. Figure 5 (a) and (b) show the surface of the carbon after the deposition of the Au nanoparticles at pH 9.5. The coverage of the support appears uniform, with nanoparticles in the range < 100 nm. Some aggregates were also spotted (not shown). Figure 5 (c) shows the energy dispersive X-ray (EDX) spectra of the synthesized AuNP/C composite, confirming that the Au nanoparticles are supported on the carbon matrix. The peaks of O and Cl elements are residues from the synthesis and/or functional groups of the carbon support.

More detailed information about the size and distribution of the Au nanoparticles across the support was obtained by HAADF-STEM characterization. Figure 6 (a) shows a HAADF-STEM image of the Au nanoparticles deposited onto the activated carbon. This investigation confirms that the Au nanoparticles are reasonably homogeneously distributed across the activated carbon (as was already suggested by SEM analysis). The particle size distribution was determined and is shown in Figure 6 (b). This shows that the mean particle size is 6.9 nm with a standard deviation of 2.8 nm. Figure 6 (a) shows that the Au nanoparticles are well spread out across the entire support. Some sporadic larger nanoparticles in the range of 50–100 nm can also be observed (see Figure S3 for their particle size distribution).

Electron tomography was utilized for complete 3D characterization. This involves the acquisition of images at various projection angles allowing for visualization of the materials in 3D and therefore the determination of whether or not the Au nanoparticles are situated inside of the activated carbon, or are simply deposited onto the surface. Figure 7 shows an ortho-slice taken from the 3D reconstruction in the xz direction, approximately halfway through the volume of the Au/C. This ortho-slice shows the presence of Au NPs (in the middle of the activated carbon). Therefore, it can be concluded that the particles are situated inside of the pores of the carbon support.

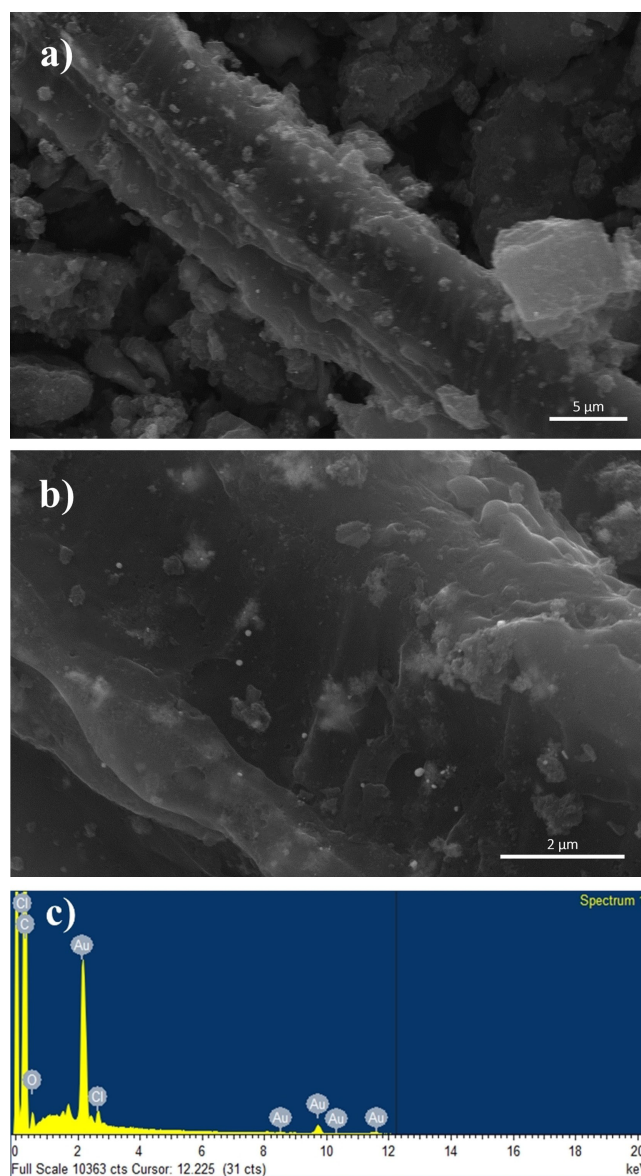


Figure 5. SEM images, (a) and (b), and EDX spectra (c) of the Au nanoparticles deposited on carbon synthesized at the optimized pH of 9.5 (9.3% loading).

This was further confirmed by comparing the total surface area of the bare Norit SX1G support (i.e., 1000 m²g⁻¹ according to the product data sheet) with that of AuNP@Norit, which showed a significant decrease to 517 m²g⁻¹. This is a further indication that the Au NPs are present in the pores and blocking them (*vide infra*).

Energy-dispersive X-ray spectroscopy (EDX) maps were acquired from various areas of the sample to determine the composition, and confirm that there are Au NPs deposited on carbon. Figure 8 shows a HAADF-STEM image and the respective elemental maps for Au and C, obtained on a representative area of the sample. The results clearly indicate the presence of Au nanoparticles, homogeneously spread across the carbon matrix, with a low degree of agglomeration. The presence of Cu

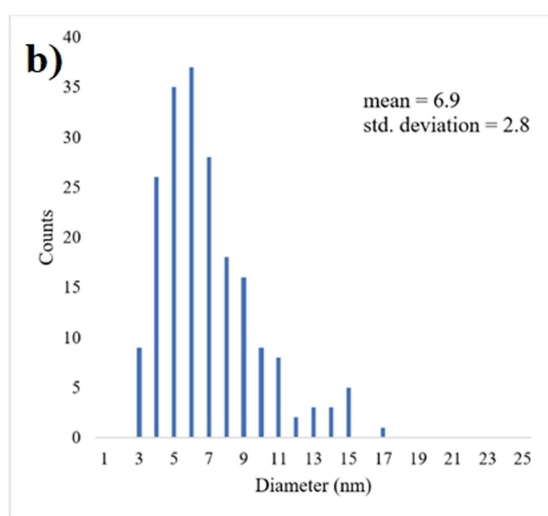
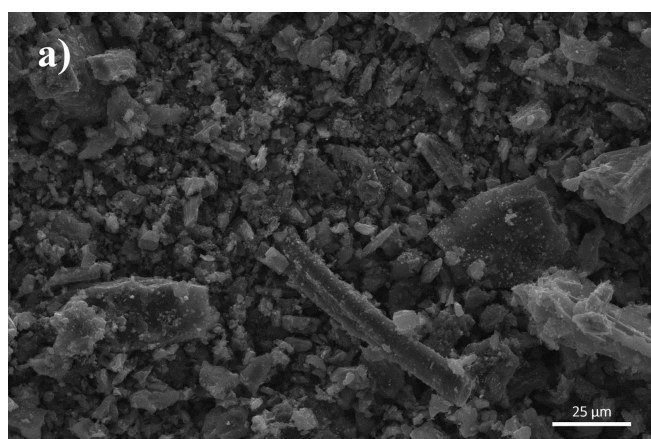


Figure 6. (a) HAADF-STEM image of the 9.3 wt % Au nanoparticles on activated carbon and (b) a histogram showing the particle size distribution of the nanoparticles for this sample.

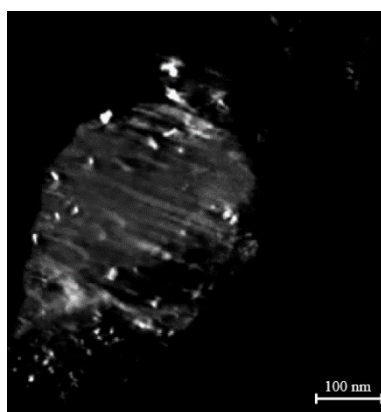


Figure 7. Ortho-slice in the xz direction approximately halfway through the volume of of Au/C sample at pH 9.5 (9.3% loading).

in the spectrum is due to the Cu grid and holder used for these measurements.

Catalytic activity testing

The very high specific EASA which was found for the AuNP/C catalyst, 282.4 m²/g, is mainly ascribed, in addition to the Au loading, to the Au nanoparticles size and homogeneous spread onto the activated carbon support, which has a particularly high specific surface area, most of which is concentrated inside its pores (ca 99.8%). A high EASA, typically boosts electrons transfer and mass transport of reactants and intermediates, leading to enhanced electrocatalytic activity.^[73]

To understand the electrocatalytic activity of the as-synthesized AuNP/C@GC catalyst towards gluconic acid oxidation, a cyclic voltammogram was recorded at ambient temperature, with a stirring velocity of 700 rpm, in 0.1 M NaOH (pH 13) with increasing amount of gluconic acid (Figure 9).

As expected, no oxidation peaks are observed in the cyclic voltammogram in the blank solution while, when gluconic acid is added, a small oxidation peak characterized by a left shoulder appears between 1 and 2 V_{RHE}, which was found, in our previous study, to be specific for the oxidation of the hydroxymethyl group on C6 in the gluconic acid molecule on gold.^[66] Thus, the increase of current density with the concentration of gluconic acid in solution indicates reaction of the substrate with the gold active sites in this potential range. However, the current density reaches a maximum of only ca 0.08 mAcm⁻². Considering the high value of EASA of this catalyst (39.5 cm²), we expected to observe a much higher electrocatalytic activity, and thus current density, at this potentials. Indeed, in our previous studies, we measured a similar current density, in the range of 0.22 mAcm⁻² (in respect to the EASA), using a bare gold flat electrode with an EASA of only 0.702 cm².^[66,67] Unfortunately, a 10² increase in EASA did not result in an increase in activity. To understand if a deactivation process was responsible for the limited reactivity of the catalyst, we recalculated the EASA of the catalyst after cycling it in a gluconic acid solution. The measurement of the EASA was repeated on the catalyst after cyclic voltammetry in 0.05 M gluconic acid and 0.1 M NaOH, and the result remained unchanged, proving that it does not get deactivated. In addition, particle size upon electrochemical cycling also does not alter (see S4), which leaves only one reasonable explanation for the low electrocatalytic activity that is detected. Indeed, based on the 3D reconstruction (*vide supra*) we believe that the substrate, gluconic acid (molecule size ~1 nm^[88,89]), cannot access the majority of the electroactive surface area of the catalyst, located inside the micropores (<2 nm) of the activated carbon.^[90] In fact, micropores are only able to absorb gases and most solvents, while mesopores (=2–50 nm) can absorb larger molecules.^[91] In this case, the EASA available for the reaction is only a small fraction (i.e. external surface area of our carbon substrate) of the total calculated EASA, which means it becomes close to that of the flat electrode. Even more so, taking this into account utilizing the AuNP/C catalyst does not result in an increase of the EASA available for the reaction, and is thus in line with the current density obtained here.

As a proof of concept, we performed the reaction in a flow reactor configuration where mass transfer limitations are

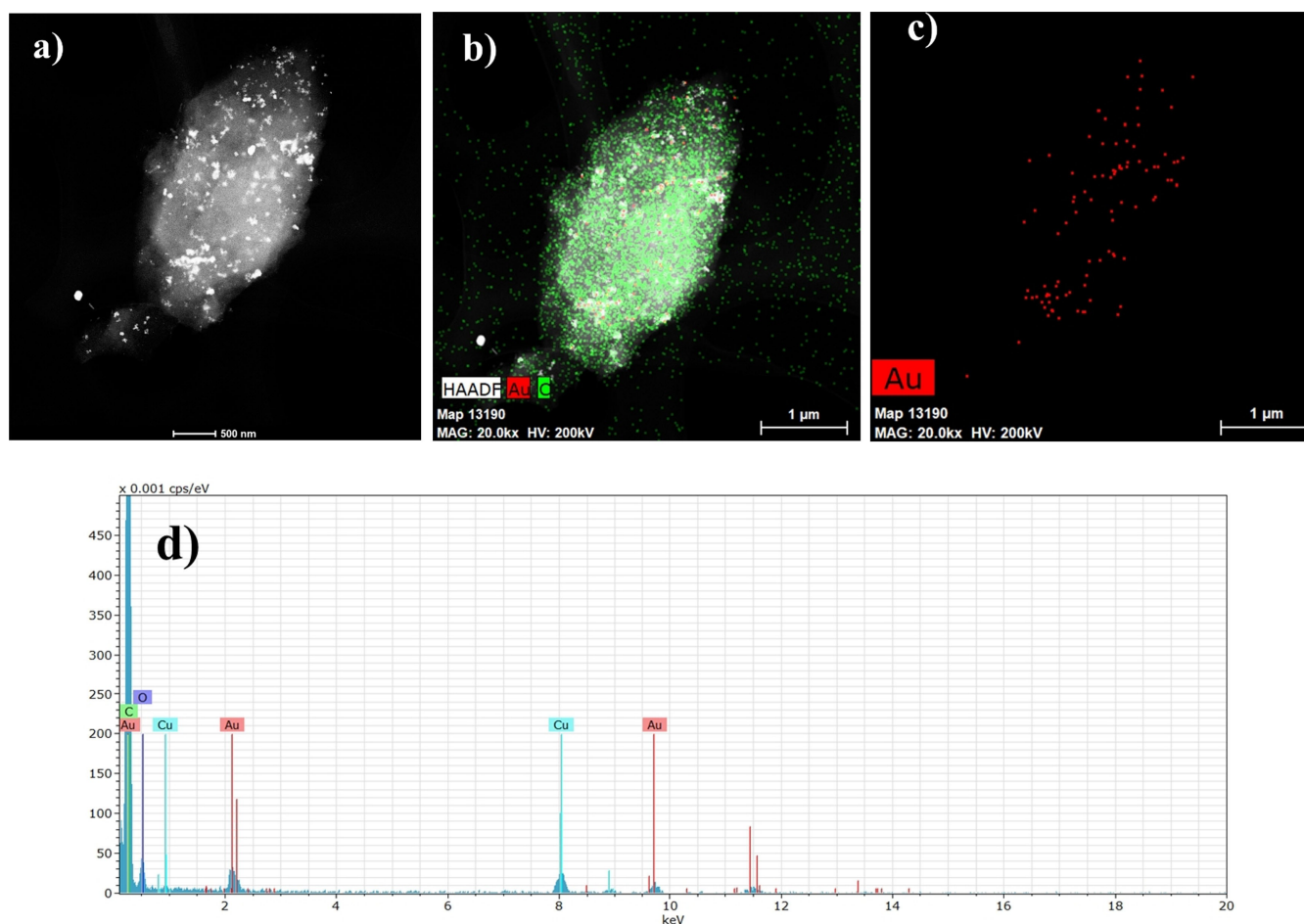


Figure 8. (a) HAADF-STEM image, (b, c) the respective EDX elemental distributions and (d) an EDX spectrum showing which elements are present for the Au/C composite with 9.3% Au-loading. For the EDX maps, Au is marked in red and C in green.

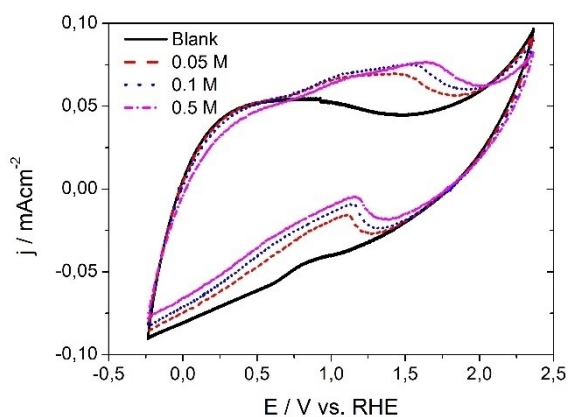


Figure 9. Voltammograms of AuNP/C@GC electrode in 0.1 M NaOH recorded at 50 mVs⁻¹, at 20 °C and stirring the solution at 700 rpm, with increasing amount of gluconic acid (from 0 to 0.5 M).

excluded. For the continuous flow experiments, we used the reactor setup described in the Experimental section with the synthesized AuNP/C dispersed over a Ti felt as catalyst, with a total EASA of 919.3 cm². In first instance, cyclic voltammetry experiments were performed at increasing concentrations of gluconic acid. Figure 10 presents the current density vs.

concentration of gluconic acid obtained at a fixed potential of 1.7 V_{RHE}, corresponding to the oxidation peak, at a flow rate of 20 mL min⁻¹ and a scan rate of 20 mVs⁻¹, utilizing a 0.1 M NaOH solution. For comparison, we report the results obtained for the AuNP/C@Ti system, as well as the Ti felt alone, to confirm that it does not contribute to the reaction.

The data clearly show that, upon addition of gluconic acid, the current density has only a slight increase, of ca 1 mA cm⁻², and that it does not increase further when the concentration of gluconic acid in solution is raised. This confirms the results obtained in the batch cell, where only a small part of gluconic acid is able to reach the gold active sites for reaction as saturation is quickly achieved here as well (no further increase in current density after adding only small amounts of gluconic acid). Despite the contribution of the higher convection given by the continuous flow, the mass transfer inside the pores of the carbon matrix remains hindered, as such limiting the reaction. Control experiments were also conducted at higher flow rates (> 20 mL min⁻¹), but no difference was observed. Given the very small difference in current density between the blank solution and the solutions containing gluconic acid, we can again assume that the reaction is only happening on the gold active sites that are situated outside the pores.

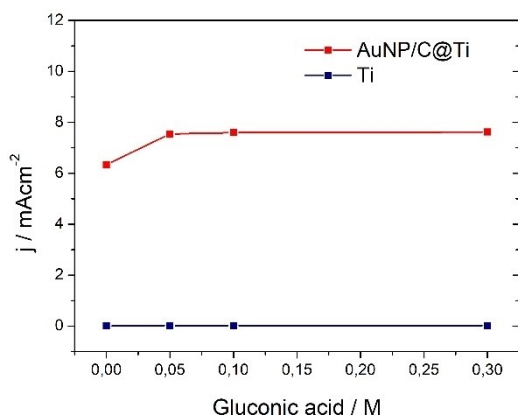


Figure 10. Plot current density vs. gluconic acid concentration obtained extracting the current density values at fixed potential of $1.7 V_{\text{RHE}}$ (corresponding to the oxidation peak) from the cyclic voltammetry study of AuNP/C@Ti (red line) and Ti felt alone (blue line) at 20 mVs^{-1} , 20°C and 20 mL min^{-1} , from a starting solution 0.1 M NaOH .

As a proof of concept, long-term electrolysis experiments were conducted applying a constant current density, and the product solutions were analyzed by HPLC. The results of chronopotentiometry experiments conducted at 10, 20 and 30 mA cm^{-2} , in a solution of 0.05 M gluconic acid and 0.1 M NaOH are shown in Figure 11.

The chronopotentiometry experiments confirm that when applying such high current density, the only reaction that occurs at the surface of the AuNP/AC@Ti electrode is the O_2 evolution reaction, which, in fact, takes place at these high potentials, and which was also evidenced by the heavy formation of bubbles at the anode, confirmed to be O_2 by gas chromatography (GC) measurements.

Chromatographic analysis of the liquid product stream revealed what we expected: no glucaric acid or relevant amount of oxidation products is detected (S5).

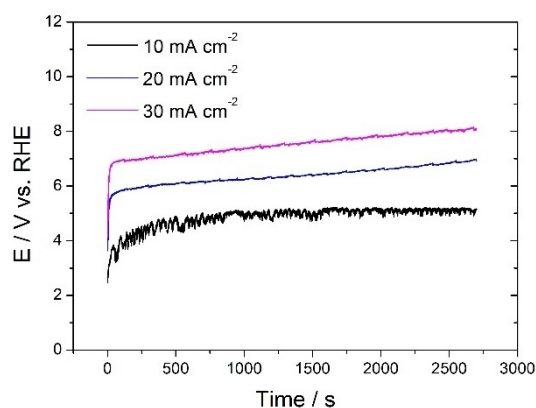


Figure 11. Results of chronopotentiometry experiments conducted at constant current densities of 10, 20 and 30 mA cm^{-2} in the flow cell, in a solution with 0.05 M gluconic acid and 0.1 M NaOH . At these currents, the O_2 evolution reaction takes place, as evidenced by the high potentials (y-axis) and the increasing O_2 bubbles formation with the current density at the anode.

In conclusion, in this work, we used an efficient synthesis method to produce an Au-based catalyst with very high EASA at low metal loading. The main advantages of this synthesis are its simplicity and an optimal Au utilization (up to 93%), with only 7% being lost during the different synthesis steps. This result was achieved by maximizing the interaction between the metallic precursor, the Au cations, and the carbonaceous support, activated carbon (Norit), during the immobilization step, by fine-tuning the pH of the synthesis broth. At pH 9.5 the maximum amount of gold was deposited on the Norit, resulting in a final loading of 9.3 wt%. Physical characterization revealed the successful deposition of very small nanoparticles, of average size between 5 and 20 nm, and their homogeneous distribution inside the micropores of the AC. The specific EASA of the catalyst was found to be as high as $282.43 \text{ m}^2 \text{ g}_{\text{Au}}^{-1}$, which is higher than typical values found in literature.^[13,15,63] The as-synthesized catalytic system was tested for the electrooxidation of gluconic acid in alkaline media in an attempt to boost the productivity of glucaric acid exploiting its very high EASA. However, cyclic voltammetry experiments conducted both, in batch and in continuous flow reactor configurations, revealed a very limited reactivity towards gluconic acid oxidation, evidenced by the low current density registered at the gluconic acid oxidation peak. Given the high EASA found, the low current density detected could only be explained assuming that gluconic acid was reacting only with a small fraction of the total gold active sites, the ones more easily accessible and present at the external surface. The explanation for this behaviour was attributed to a difficult diffusion of the reagent inside the catalyst nanopores. Gluconic acid, like glucose, is a rather bulky molecule with a relatively low diffusivity compared to other, smaller, organic molecules.^[92] This spatial hindrance prevented gluconic acid to penetrate inside the pores of the catalyst, leaving, as only accessible active sites, the Au nanoparticles situated outside the pores of the carbon matrix. Three evidences were given to explain this phenomena: 1) most of the EASA of the synthesized catalyst is located inside the pores of the carbon matrix (as evidenced by TEM tomography), as the area inside the pores can go up to 99.8% of the total available surface of the carbon support. This would result in an accessible EASA of only 0.2% of the total, corresponding to ca 0.079 cm^2 for the catalytic system used in the batch cell and 1.838 cm^2 for the one used in the flow cell, which are close to the value found for the flat Au electrode (0.702 cm^2) and would thus explain the low performance; 2) while gluconic acid electrooxidation appeared to be very limited at the AuNP/C electrode, O_2 evolution reaction seemed to proceed favourably, as evidenced by the heavy formation of O_2 bubbles, which increased with applied increasing current density. Moreover, O_2 bubbles formation did not occur in absence of AuNP as activated carbon itself is an inert material, which is why it finds application in catalysis as carrier of an active phase (most of the times noble metals).^[93] In fact, it is because of its inertness and high degree of microporosity that activated carbon has been found particularly suitable for application as support for precious metals and other catalytic active compounds for oxygen electroreduction reaction (OER);^[93–97] and 3) a final proof was

given by the procedure used to measure the Au loading in the AuNP/C catalyst by ICP-MS. Here, the reagent used to dissolve gold was also unable to access the Au situated inside the pores of the carbon matrix.

Conclusions

The efficient synthesis of a gold catalyst made of gold nanoparticles deposited onto the surface of activated carbon was achieved by a wet impregnation method at an optimal pH of the bath of 9.5, critical in determining the gold-carbon interaction, with a resulting loading of 9.3% and an Au utilization as high as 93%. The catalyst was characterized by SEM-EDX and HAADF-STEM electron tomography, showing a very uniform coverage of the carbon matrix with the Au nanoparticles, whose size ranged between 5 and 20 nm. The catalytic system was tested for the electrooxidation of gluconic acid in alkaline media in an attempt to boost the productivity of glucaric acid by exploiting its very high specific EASA, which was calculated to be as high as $282.43 \text{ m}^2 \text{ g}_{\text{Au}}^{-1}$, which is 10^2 times higher than that found for the Au bulk electrode used for our previous studies. However, it was found that the catalyst is not designed for reactions involving bulky molecules such as sugars and its derivatives, while it would be a good fit for application in reactions involving small molecules (i.e. gasses as O_2) making it a potential candidate for reactions involving molecules with high diffusivity as CO_2 , CH_4 , N_2 . In particular, such high performance Au-based catalyst could be a very good fit for application in the nitrogen reduction reaction (NRR), where gold is known to achieve the highest selectivity,^[98,99] which will be the subject of our further investigations. From our findings, we believe that catalytic systems in which gold is directly deposited onto the surface of high surface area supports characterized by large porosity as felts, nets, etc, would make a better choice for the electrooxidation of glucose/gluconic acid.

Acknowledgements

The research described in this article has not been supported by the Climate, Infrastructure and Environment Executive Agency of the European Commission. The views expressed in this article have not been adopted or in any way approved by the European Commission and do not constitute a statement of the European Commission's views.

S. Hoekx was supported by Research Foundation Flanders (FWO 1542623N). The authors would like to thank Prof. Dr. Christophe Vande Velde, University of Antwerp, for the XRD analysis.

Conflict of Interests

The authors declare no conflict of interest.

Data Availability Statement

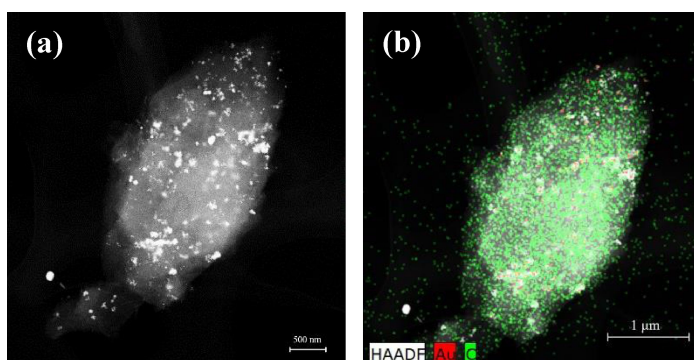
The data that support the findings of this study are available from the corresponding author upon reasonable request.

Keywords: electrocatalysis · gold · glucaric acid · gold nanoparticles · electroactive surface area

- [1] S. Ghosh, Y. Holade, H. Remita, K. Servat, P. Beaunier, A. Hagège, K. B. Kokoh, T. W. Napporn, *Electrochim. Acta* **2016**, *212*, 864–875.
- [2] M. T. Jeena, T. Bok, S. H. Kim, S. Perk, J. Y. Kim, S. Park, J. H. Ryu, *Nanoscale* **2016**, *8*, 9245–9253.
- [3] Q. Zhang, E. Uchaker, S. L. Candelaria, G. Cao, *Chem. Soc. Rev.* **2013**, *42*, 3127–3171.
- [4] S. Ghosh, A. L. Teillout, D. Floresyona, P. De Oliveira, A. Hagège, H. Remita, *Int. J. Hydrogen Energy* **2015**, *40*, 4951–4959.
- [5] T. F. Chu, R. Rajendran, I. Kuznetsova, G. J. Wang, *J. Power Sources* **2020**, *453*, 227844.
- [6] H. F. Cui, J. S. Ye, X. Liu, W. De Zhang, F. S. Sheu, *Nanotechnology* **2006**, *17*, 2334.
- [7] S. Ben Aoun, I. Taniguchi, *Chem. Lett.* **2008**, *37*, 936–937.
- [8] D. Basu, S. Basu, *Int. J. Hydrogen Energy* **2011**, *36*, 14923–14929.
- [9] D. Choukroun, N. Daems, T. Kenis, T. Van Everbroeck, J. Hereijgers, T. Altantzis, S. Bals, P. Cool, T. Breugelmanns, *J. Phys. Chem. C* **2020**, *124*, 1369–1381.
- [10] S. P. Tung, T. K. Huang, C. Y. Lee, H. T. Chiu, *RSC Adv.* **2012**, *2*, 1068–1073.
- [11] J. Ustarroz, B. Geboes, H. Vanrompay, K. Sentosun, S. Bals, T. Breugelmanns, A. Hubin, *ACS Appl. Mater. Interfaces* **2017**, *9*, 16168–16177.
- [12] B. Geboes, J. Ustarroz, K. Sentosun, H. Vanrompay, A. Hubin, S. Bals, T. Breugelmanns, *ACS Catal.* **2016**, *6*, 5856–5864.
- [13] B. Geboes, I. Mintsouli, B. Wouters, J. Georgieva, A. Kakaroglou, S. Sotiropoulos, E. Valova, S. Armanyanov, A. Hubin, T. Breugelmanns, *Appl. Catal. B* **2014**, *150–151*, 249–256.
- [14] L. Yan, A. Brouzgou, Y. Meng, M. Xiao, P. Tsiakaras, S. Song, *Appl. Catal. B* **2014**, *150–151*, 268–274.
- [15] J. T. Steven, V. B. Golovko, B. Johannessen, A. T. Marshall, *Electrochim. Acta* **2016**, *187*, 593–604.
- [16] C. Li, O. J. H. Chai, Q. Yao, Z. Liu, L. Wang, H. Wang, J. Xie, *Mater. Horiz.* **2021**, *8*, 1657–1682.
- [17] L. Yu, L. Zhang, X. Zhang, G. Dai, J. Zhang, X. Wang, H. You, *ACS Appl. Energ. Mater.* **2020**, *3*, 723–732.
- [18] Z. Liang, L. Song, S. Deng, Y. Zhu, E. Stavitski, R. R. Adzic, J. Chen, J. X. Wang, *J. Am. Chem. Soc.* **2019**, *141*, 9629–9636.
- [19] V. Celorrio, P. M. Quaino, E. Santos, J. Flórez-Montaño, J. J. L. Humphrey, O. Guillén-Villafuerte, D. Plana, M. J. Lázaro, E. Pastor, D. J. Fermín, *ACS Catal.* **2017**, *7*, 1673–1680.
- [20] M. Zhou, C. Zeng, Y. Chen, S. Zhao, M. Y. Sfeir, M. Zhu, R. Jin, *Nat. Commun.* **2016**, *7*, 1–7.
- [21] Y. Lu, C. Zhang, X. Li, A. R. Frojd, W. Xing, A. Z. Clayborne, W. Chen, *Nano Energy* **2018**, *50*, 316–322.
- [22] B. Liu, H. Yao, W. Song, L. Jin, I. M. Mosa, J. F. Rusling, S. L. Suib, J. He, *J. Am. Chem. Soc.* **2016**, *138*, 4718–4721.
- [23] W. Chen, S. Chen, *Angew. Chem. Int. Ed.* **2009**, *48*, 4386–4389.
- [24] S. Zhao, R. Jin, H. Abroshan, C. Zeng, H. Zhang, S. D. House, E. Gottlieb, H. J. Kim, J. C. Yang, R. Jin, *J. Am. Chem. Soc.* **2017**, *139*, 1077–1080.
- [25] L. Wang, Z. Tang, W. Yan, H. Yang, Q. Wang, S. Chen, *ACS Appl. Mater. Interfaces* **2016**, *8*, 20635–20641.
- [26] T. C. Jones, L. Sumner, G. Ramakrishna, M. Bin Hatshan, A. Abuhagr, S. Chakraborty, A. Dass, *J. Phys. Chem. C* **2018**, *122*, 17726–17737.
- [27] F. Paquin, J. Rivnay, A. Salleo, N. Stingelin, C. Silva, *J. Mater. Chem. C* **2015**, *3*, 10715–10722.
- [28] D. Alba-Molina, A. R. Puente Santiago, J. J. Giner-Casares, E. Rodríguez-Castellón, M. T. Martín-Romero, L. Camacho, R. Luque, M. Cano, *J. Mater. Chem. A* **2019**, *7*, 20425–20434.
- [29] M. S. El-Deab, T. Ohsaka, *Electrochem. Commun.* **2002**, *4*, 288–292.
- [30] M. Valenti, N. P. Prasad, R. Kas, D. Bohra, M. Ma, V. Balasubramanian, L. Chu, S. Gimenez, J. Bisquert, B. Dam, W. A. Smith, *ACS Catal.* **2019**, *9*, 3527–3536.
- [31] X. Ma, Y. Shen, S. Yao, C. An, W. Zhang, J. Zhu, R. Si, C. Guo, C. An, *J. Mater. Chem. A* **2020**, *8*, 3344–3350.

- [32] M. Cho, J. M. Kim, B. Kim, S. Yim, Y. J. Kim, Y. S. Jung, J. Oh, *J. Mater. Chem. A* **2019**, *7*, 6045–6052.
- [33] M. M. Shi, D. Bao, B. R. Wulan, Y. H. Li, Y. F. Zhang, J. M. Yan, Q. Jiang, *Adv. Mater.* **2017**, *29*, 2–7.
- [34] F. Zhou, L. M. Azofra, M. Ali, M. Kar, A. N. Simonov, C. McDonnell-Worth, C. Sun, X. Zhang, D. R. Macfarlane, *Energy Environ. Sci.* **2017**, *10*, 2516–2520.
- [35] J. Wang, L. Yu, L. Hu, G. Chen, H. Xin, X. Feng, *Nat. Commun.* **2018**, *9*, DOI 10.1038/s41467-018-04213-9.
- [36] W. Zhang, Y. Shen, F. Pang, D. Quek, W. Niu, W. Wang, P. Chen, *ACS Appl. Mater. Interfaces* **2020**, *12*, 41613–41619.
- [37] H. Boo, S. Park, B. Ku, Y. Kim, J. H. Park, H. C. Kim, T. D. Chung, *J. Am. Chem. Soc.* **2004**, *126*, 4524–4525.
- [38] Y. Y. Song, D. Zhang, W. Gao, X. H. Xia, *Chem. Eur. J.* **2005**, *11*, 2177–2182.
- [39] A. Chen, X. Peng, K. Koczur, B. Miller, *Chem. Commun.* **2004**, 1964–1965.
- [40] J. C. Thorp, K. Sieradzki, L. Tang, P. A. Crozier, A. Misra, M. Nastasi, D. Mitlin, S. T. Picraux, *Appl. Phys. Lett.* **2006**, *88*, 1–3.
- [41] J. Wang, D. F. Thomas, A. Chen, *Anal. Chem.* **2008**, *80*, 997–1004.
- [42] J. Kimling, M. Maier, B. Okenve, V. Kotaidis, H. Ballot, A. Plech, *J. Phys. Chem. B* **2006**, *110*, 15700–15707.
- [43] L. He, M. D. Musick, S. R. Nicewarner, F. G. Salinas, S. J. Benkovic, M. J. Natan, C. D. Keating, *J. Am. Chem. Soc.* **2000**, *122*, 9071–9077.
- [44] M. Nazemi, S. R. Panikkanvalappil, M. A. El-Sayed, *Nano Energy* **2018**, *49*, 316–323.
- [45] H. Lv, L. Sun, X. Chen, D. Xu, B. Liu, *Green Chem.* **2019**, *21*, 2043–2051.
- [46] M. H. Naveen, N. G. Gurudatt, H. B. Noh, Y. B. Shim, *Adv. Funct. Mater.* **2016**, *26*, 1590–1601.
- [47] Y. Y. Peng, D. Guo, W. Ma, Y. T. Long, *ChemElectroChem* **2018**, *5*, 2982–2985.
- [48] L. Nahar, A. A. Farghaly, R. J. A. Esteves, I. U. Arachchige, *Chem. Mater.* **2017**, *29*, 7704–7715.
- [49] L. Y. Chen, N. Chen, Y. Hou, Z. C. Wang, S. H. Lv, T. Fujita, J. H. Jiang, A. Hirata, M. W. Chen, *ACS Catal.* **2013**, *3*, 1220–1230.
- [50] J. Wang, F. Chen, Y. Jin, R. L. Johnston, *ChemSusChem* **2018**, *11*, 1354–1364.
- [51] L. Yuan, Z. Yan, L. Jiang, E. Wang, S. Wang, G. Sun, *J. Energy Chem.* **2016**, *25*, 805–810.
- [52] Y. Li, W. Ding, M. Li, H. Xia, D. Wang, X. Tao, *J. Mater. Chem. A* **2015**, *3*, 368–376.
- [53] B. K. Jena, C. R. Raj, *Langmuir* **2007**, *23*, 4064–4070.
- [54] S. Karra, M. Wooten, W. Griffith, W. Gorski, *Electrochim. Acta* **2016**, *218*, 8–14.
- [55] Q. Xue, J. Bai, C. Han, P. Chen, J. X. Jiang, Y. Chen, *ACS Catal.* **2018**, *8*, 11287–11295.
- [56] D. Bao, Q. Zhang, F. L. Meng, H. X. Zhong, M. M. Shi, Y. Zhang, J. M. Yan, Q. Jiang, X. B. Zhang, *Adv. Mater.* **2017**, *29*, 1–5.
- [57] J. Wang, F. Chen, Y. Jin, Y. Lei, R. L. Johnston, *Adv. Funct. Mater.* **2017**, *27*, 1–10.
- [58] W. Jiao, C. Chen, W. You, G. Chen, S. Xue, J. Zhang, J. Liu, Y. Feng, P. Wang, Y. Wang, H. Wen, R. Che, *Appl. Catal. B* **2020**, *262*, 118298.
- [59] S. Hebié, Y. Holade, K. Servat, B. K. Kokoh, T. W. Napporn, *Catal. Appl. Nano-Gold Catal.* **2016**, DOI 10.5772/64770.
- [60] H. Yin, H. Tang, D. Wang, Y. Gao, Z. Tang, *ACS Nano* **2012**, *6*, 8288–8297.
- [61] S. Zhao, R. Jin, Y. Song, H. Zhang, S. D. House, J. C. Yang, R. Jin, *Small* **2017**, *13*, 1–7.
- [62] Y. Yu, Y. Gao, K. Hu, P. Y. Blanchard, J. M. Noël, T. Nareshkumar, K. L. Phani, G. Friedman, Y. Gogotsi, M. V. Mirkin, *ChemElectroChem* **2015**, *2*, 58–63.
- [63] L. Yang, Y. Zhang, M. Chu, W. Deng, Y. Tan, M. Ma, X. Su, Q. Xie, S. Yao, *Biosens. Bioelectron.* **2014**, *52*, 105–110.
- [64] J. Snyder, P. Asanithi, A. B. Dalton, J. Erlebacher, *Adv. Mater.* **2008**, *20*, 4883–4886.
- [65] F. Xie, Z. Huang, C. Chen, Q. Xie, Y. Huang, C. Qin, Y. Liu, Z. Su, S. Yao, *Electrochem. Commun.* **2012**, *18*, 108–111.
- [66] G. Moggia, T. Kenis, N. Daems, T. Breugelmans, *ChemElectroChem* **2020**, *7*, e1901592.
- [67] G. Moggia, J. Schalck, N. Daems, T. Breugelmans, *Electrochim. Acta* **2021**, *374*, 137852.
- [68] D. Bin, H. Wang, J. Li, H. Wang, Z. Yin, J. Kang, B. He, Z. Li, *Electrochim. Acta* **2014**, *130*, 170–178.
- [69] H. Guzmán, F. Zammillo, D. Roldán, C. Galletti, N. Russo, S. Hernández, *Catalysts* **2021**, *11*(4), 482.
- [70] C. F. C. Lim, D. A. Harrington, A. T. Marshall, *Electrochim. Acta* **2017**, *238*, 56–63.
- [71] S. L. Gojković, *J. Electroanal. Chem.* **2004**, *573*, 271–276.
- [72] I. Dumitrescu, R. M. Crooks, *Proc. Natl. Acad. Sci. USA* **2012**, *109*, 11493–11497.
- [73] S. A. N. Md Rahim, C. S. Lee, F. Abnisa, W. M. A. Wan Daud, M. K. Aroua, P. Cognet, Y. Pérès, *Chemosphere* **2022**, *295*, 133949.
- [74] N. N. Bv, “Norit SX 1 G,” **2011**.
- [75] S. Hermans, A. Deffernez, M. Devillers, *Appl. Catal. A* **2011**, *395*, 19–27.
- [76] S. Hermans, A. Deffernez, M. Devillers, *Catal. Today* **2010**, *157*, 77–82.
- [77] A. Deffernez, S. Hermans, M. Devillers, *J. Phys. Chem. C* **2007**, *111*, 9448–9459.
- [78] E. Irtem, D. Arenas Esteban, M. Duarte, D. Choukroun, S. Lee, M. Ibáñez, S. Bals, T. Breugelmans, *ACS Catal.* **2020**, *10*, 13468–13478.
- [79] W. Albrecht, S. Bals, *J. Phys. Chem.* **2020**, *124*, 27276–27286.
- [80] T. K. Moon, *IEEE Signal Process. Mag.* **1996**, *13*, 47–60.
- [81] M. Duarte, J. Hereijgers, N. Daems, S. Van Daele, T. Breugelmans, *J. Environ. Chem. Eng.* **2022**, *10*, 107836.
- [82] Y. Wang, T. S. Nguyen, X. Liu, X. Wang, *J. Power Sources* **2010**, *195*, 2619–2622.
- [83] E. Auer, A. Freund, J. Pietsch, T. Tacke, *Appl. Catal. A* **1998**, *173*, 259–271.
- [84] X. Hao, L. Quach, J. Korah, W. A. Spieker, J. R. Regalbuto, *J. Mol. Catal. A* **2004**, *219*, 97–107.
- [85] P. J. M. Carrott, J. M. V. Nabais, M. M. L. Ribeiro Carrott, J. A. Menéndez, *Microporous Mesoporous Mater.* **2001**, *47*, 243–252.
- [86] K. Sneha, M. Sathishkumar, S. Kim, Y. S. Yun, *Process Biochem.* **2010**, *45*, 1450–1458.
- [87] S. Krishnamurthy, A. Esterle, N. C. Sharma, S. V. Sahi, *Nanoscale Res. Lett.* **2014**, *9*, 627.
- [88] W. W. LaMorte, “From Molecules to Man - A perspective on size,” can be found under [https://sphweb.bumc.bu.edu/otlt/mph-modules/ph/ph709_basicecellbiology/ph709_basicecellbiology8.html#:~:text=A Perspective on Size,-An angstrom is&text=A glucose molecule is about 9 angstroms,2016](https://sphweb.bumc.bu.edu/otlt/mph-modules/ph/ph709_basicecellbiology/ph709_basicecellbiology8.html#:~:text=A%20Perspective%20on%20Size,-An%20angstrom%20is%20A%20glucose%20molecule%20is%20about%209%20angstroms,2016).
- [89] “HOW BIG ARE BIOCHEMICAL NUTS AND BOLTS?,” can be found under <http://book.bionumbers.org/how-big-are-biochemical-nuts-and-bolts/,n.d>.
- [90] M. Ilomuanya, B. Nashiru, N. Ifudu, C. Igwilo, *J. Microsc. Ultrastruct.* **2017**, *5*, 32.
- [91] H. W. Annemieke, Modification and Application of Carbon Supported Noble Metal Catalysts, **2000**.
- [92] D. Basu, S. Basu, *Electrochim. Acta* **2010**, *55*, 5775–5779.
- [93] W. M. T. M. Reimerink, *The Use of Activated Carbon as Catalyst and Catalyst Carrier in Industrial Applications*, Elsevier Masson SAS, **1999**.
- [94] K. Chandrasekhar, *Effective and Nonprecious Cathode Catalysts for Oxygen Reduction Reaction in Microbial Fuel Cells*, Elsevier B. V., **2018**.
- [95] P. Thangavel, G. Kim, K. S. Kim, *J. Mater. Chem. A* **2021**, *9*, 14043–14051.
- [96] S. Sekar, D. Y. Kim, S. Lee, *Nanomaterials* **2020**, *10*, 1–13.
- [97] K. Kordek, H. Yin, P. Rutkowski, H. Zhao, *Int. J. Hydrogen Energy* **2019**, *44*, 23–33.
- [98] X. Guo, H. Du, F. Qu, J. Li, *J. Mater. Chem. A* **2019**, *7*, 3531–3543.
- [99] S. K. Sahoo, J. Heske, M. Antonietti, Q. Qin, M. Oschatz, T. D. Ku, **2020**, *3*, 10061–10069.

Manuscript received: June 23, 2023
Revised manuscript received: July 31, 2023
Version of record online: ■■■, ■■■



Electrocatalysis: Gold nanoparticles with diameter between 5 and 20 nm evenly distributed onto porous activated carbon (Norit) were obtained using a facile “one-pot” chemical synthesis technique with very high metal utilization. The AuNP/C nanocomposite was characterized using SEM, HAADF-STEM electron to-

mography and electrochemical techniques, revealing a very large electroactive surface area (EASA). The figure shows the HAADF-STEM image (a) and the respective EDX elemental distribution (b) for the AuNP/C composite with 9.3% Au-loading developed in this work (Au is marked in red and C in green).

G. Moggia*, S. Hoekx, Dr. N. Daems, Prof. Dr. S. Bals, Prof. Dr. T. Breugelmans

1 – 11

Synthesis and Characterization of a Highly Electroactive Composite Based on Au Nanoparticles Supported on Nanoporous Activated Carbon for Electrocatalysis

